Hue University Journal of Science: Natural Science
Vol. 130, No. 1B, 59–67, 2021

pISSN 1859-1388
eISSN 2615-9678

$Na_2Fe_3(SO_4)_4$ AS A NEW HIGH-VOLTAGE CATHODE MATERIAL FOR SODIUM-ION BATTERIES

Thien Lan Tran[1,2], Huu Duc Luong[3,4], Trong Lam Pham[1], Viet Bac Phung[5], Van An Dinh[1,6,7]*

[1] Nanotechnology Program, VNU Vietnam Japan University, Luu Huu Phuoc St., My Dinh I, Hanoi, Vietnam
[2] Department of Physics, Hue University of Education, Hue University, 34 Le Loi St., Hue, Vietnam
[3] Division of Precision Science & Technology and Applied Physics, Graduate School of Engineering, Osaka University, Suita, Osaka 565-0871, Japan
[4] Department of Theoretical Nanotechnology, The Institute of Scientific and Industrial Research, Osaka University, Suita, Osaka 565-0871, Japan
[5] Institute of Sustainability Science, VNU Vietnam Japan University, Luu Huu Phuoc St., My Dinh I, Hanoi, Vietnam
[6] Institute of Science and Technology Development, Thu Dau Mot University, 6 Tran Van On St., Thu Dau Mot, Binh Duong, Vietnam
[7] Department of Precision Engineering, Graduate School of Engineering, Osaka University, 2-1 Yamadaoka, Suita, Osaka 565-0871, Japan

* Correspondence to Van An Dinh <divan@pre.eng.osaka-u.ac.jp>

(*Received: 21 February 2021; Accepted: 22 March 2021*)

Abstract. Based on the density functional theory, we propose a promising cathode material, $Na_2Fe_3(SO_4)_4$, applicable for sodium-ion batteries. The crystal structure, stability, average voltage, and diffusion mechanism are carefully investigated to evaluate the electrochemical properties. The proposed material exhibits a high voltage of 4.0 V during the Na extraction. A small polaron is proved to be formed preferably at the first nearest Fe sites to Na vacancy and simultaneously accompanies the Na vacancy during its migration. Four elementary diffusion processes of the polaron–Na vacancy complexes, namely two parallel and two crossing processes, have been explored. The significant difference of activation energies between parallel and crossing processes suggests the substantial effect of the small polaron migration on the Na vacancy diffusion. We found that the parallel process along the [001] direction has the lowest activation energy of 808 meV, implying that the Na vacancy preferably diffuses in a zigzag pathway along the [001] direction.

Keywords: sodium iron sulfate, cathode material, SIBs, diffusion mechanism, DFT

1 Introduction

For recent decades, rechargeable Li-ion batteries have predominated the commercial market of the energy storage systems applicable for portable devices, such as laptops, smartphones, and cameras. The world's over-population and the environmental issues related to global warming have induced increasing energy demand for rechargeable batteries. However, the scanty global lithium reserves of only 53 megatons and the scattered distribution in a very few countries, such as China, Australia, Argentina, and Bolivia, would limit the long-term applications and cause the dramatic increase in production cost [1].

To struggle with the problems related to Li resource, researchers have performed more and more in-depth studies to develop a new positive electrode for rechargeable ion batteries, by using other elements, such as Na, K, Mg, and Al, as charge carriers. If lithium is not taken into account, sodium would be the best alternative as a charge carrier for ion batteries [2]. Sodium is the

sixth most abundant element on Earth. Sodium's weight contributes to 2.6% of the Earth's crust, ocean, and atmosphere [3]. Because sodium-based compounds are more abundant than lithium, it is expected that Na-ion batteries would have a much lower production cost. Even though Na ion has a greater ionic weight than Li ion, Na is lighter than other elements in the alkaline earth metal group. Furthermore, Na ion's radius is just 1.37 times that of Li, so Na ion can easily diffuse inside materials with a reasonable energy. Compared with analogous lithium-based compounds, sodium-based cathode materials exhibit high voltages, good capacities, and high energy densities [4]. As a result, sodium-based batteries might replace the Li-ion counterpart to become the next generation of rechargeable batteries in the commercial market in the near future.

Transition metal ions play a crucial role in the electronic structure and electrochemical properties of cathode materials, and they also contribute to the production cost of batteries. To reduce the reliance on Ni or Co compounds, researchers study other cheaper materials from abundant transition metals. Among them, iron-based materials are much cheaper than Ni- or Co-based compounds because iron is the fourth most abundant element of the Earth's crust, accounting for 4.7% of the earth's weight [3]. Various iron-based materials, such as oxides and polyanions, have been reported in many profound works. For example, Okada et al. [5] report that $NaFeO_2$ exhibit a capacity of 80 $mA{\cdot}h{\cdot}g^{-1}$ and a threshold voltage corresponding to that capacity above 3.4 V. However, due to the movement of iron atoms to occupy the adjacent Na vacancy sites when Na-ions are removed, the iron oxide frame structure would become unstable despite the highest redox pairs of Fe^{3+}/Fe^{4+}. The binary oxides $Na_x[Fe_{1/2}Mn_{1/2}]O_2$ [6] show a significantly higher capacity of 190 $mA{\cdot}h{\cdot}g^{-1}$ with a voltage ranging from 1.8 to 4.2 V. Especially, the polyanion framework compounds gain much attraction from researchers. An open-circuit voltage of 3.06 V and a capacity of 110 $mA{\cdot}h{\cdot}g^{-1}$ of Na_2FePO_4F is reported [7]. After that, $NaFePO_4$ with an operating voltage of 2.7 V with a capacity of 118 $mA{\cdot}h{\cdot}g^{-1}$ is also announced [8]. $Na_2FeP_2O_7$ [9] and $Na_4Fe_3(PO_4)_2$ (P_2O_7) [10] exhibiting an overall voltage of 3.0 and 3.2 V with a capacity of 100 $mA{\cdot}h{\cdot}g^{-1}$ have also been proposed. In 2014, Barpanda et al. [11] succeeded in synthesising a new sulfate-based compound $Na_2Fe_2(SO_4)_3$, possessing a voltage plateau at 3.8 V with high mobility of Na-ions along the [001] direction and requires low activation energy of 280 meV. From the reported data, it is noted that iron-based compounds not only have a lower production cost but also exhibit good electrochemical properties. These materials are promising for rechargeable batteries.

Replacing Fe atoms with Mn atoms in the orthorhombic $Na_2Mn_3(SO_4)_4$ compound with a high voltage of 4.48 V [12], we design a new cathode candidate applicable for sodium rechargeable batteries. Herein, we employ the density functional theory (DFT) to examine the stability, electronic and electrochemical properties, and diffusion mechanism of the proposed material. Since a small polaron would form at the transition metal sites of the transition metal-based cathode materials and might hinder the diffusion of alkali ions, we also utilize the advanced diffusion model proposed by Dinh et al. [13] to naturally and accurately describe the diffusion mechanism of alkali ions. This advanced model has been widely applied to explore the alkali vacancy-accompanied polaron complexes in various cathode materials applicable to both lithium- and sodium-ion batteries [14-21]. The effect of small polaron migration in each of the elementary diffusion processes of Na ion-accompanying polaron complexes is also carefully addressed.

pISSN 1859-1388
eISSN 2615-9678

2 Calculation scheme

All density functional theory simulations are performed by using the Projector Augmented Wave (PAW) method implemented in the Vienna *ab initio* Simulation Package (VASP) [22-25]. The Perdew-Burke-Ernzerhof (PBE) [26] generalized gradient approximation with a Hubbard-like U term (GGA+U, U_{eff} = 4.0 eV [27]) is applied to deal with 3*d* orbitals of Fe ions. Cut-off energy of 500 eV is used, and a k-point mesh of 1 × 2 × 2 is applied, corresponding to a 4 f.u. unit cell. The spin polarizations for antiferromagnetic (AFM), ferromagnetic (FM), and nonmagnetic (NM) configurations are investigated for finding out the most stable magnetic configuration. All of the optimizations converge when the residual atomic forces are less than 0.03 eV/Å. For examining the stability, the phonon spectrum is estimated by using the PHONOPY code [28] with the non-analytical correction term [29].

The open-circuit voltage is calculated according to Formula (1)

$$V = -\frac{E[\mathrm{Na}x\mathrm{Fe3(SO4)4}] - E[\mathrm{Fe3(SO4)}] - xE[\mathrm{Na}]}{xe} \quad (1)$$

where E[Na$_x$Fe$_3$(SO$_4$)$_4$], E[Fe$_3$(SO$_4$)], and E[Na] are total energies of Na$_x$Fe$_3$(SO$_4$)$_4$, Fe$_3$(SO$_4$)$_4$, and metal Na, respectively. x stands for the number of Na atoms in a chemical formula of the considered compound.

For the diffusion mechanism, the nudged elastic band (NEB) [30] calculations are performed with the spring force of − 5 eV/Å. NEB calculations converge when the atomic forces become smaller than 0.03 eV/Å.

3 Results and discussion

3.1 Crystal structure and stability

The orthorhombic crystal structure of Na$_2$Fe$_3$(SO$_4$)$_4$ (space group *Cmc*2$_1$) [12] is depicted in Fig. 1. Similar to Na$_2$Mn$_3$(SO$_4$)$_4$, a unit cell

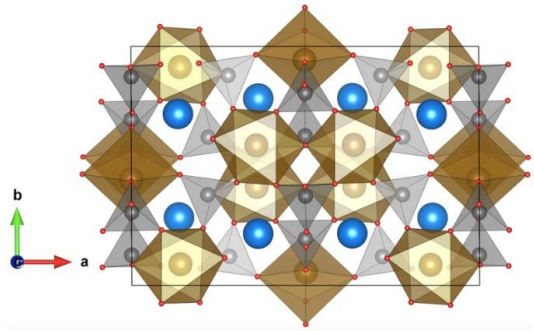

Fig. 1. Crystal structure of Na$_2$Mn$_3$(SO$_4$)$_4$. Brown, grey, blue and red balls indicate Fe, S, Na and O positions, respectively. Brown octahedra and grey tetrahedra represent FeO$_6$ and SO$_4$ groups

contains 12 distorted FeO$_6$ groups, which share their corners with other FeO$_6$ octahedra and sulfate groups SO$_4$. Along the [100] direction, two octahedra Fe^{I}O$_6$ share one oxygen corner to form a dimer [Fe$^{I}_2$O$_{11}$], linking to other dimers by sharing oxygen ions with the sulfate groups. Along the [001] direction, groups Fe^{II}O$_6$ are connected via sharing two oxygen atoms at their axial corners to form infinite wave-like [Fe^{II}O$_5$]$_\infty$ chains. The dimer [Fe$^{I}_2$O$_{11}$] group and the infinite chains [Fe^{II}O$_5$]$_\infty$ connect via the sulfate group to construct a complicated three-dimensional framework. The blank spaces function as the tunnels where sodium ions can be sheltered.

To determine the most stable magnetic configurations, we calculate the total energies of the different magnetic configurations, including antiferromagnetic (AFM), ferromagnetic (FM) and nonmagnetic (NM) orders. It is found that AFM configuration would be the most stable structure with significantly lower energy ($E_{\mathrm{FM}} - E_{\mathrm{AFM}}$ = 0.341 eV and $E_{\mathrm{NM}} - E_{\mathrm{AFM}}$ = 29.851 eV). Since AFM configuration is much more stable than the others, we employed the AFM order to examine the stability of the proposed materials.

In the literature, phonon dispersions representing the relation between frequencies' normal modes and wave vectors in a crystal are widely estimated to provide evidence of the

thermal stability of crystal structures. The phonon dispersions are estimated by using the PHONOPY code [28]. As can be seen from Fig. S1 in the Supplement, no imaginary frequency observed in the phonon spectrum implies that the proposed material exists thermodynamically.

The lattice parameters of the most stable structure are listed in Table 1. The octahedral $Fe^{I}O_6$ has the Fe^{I}–O bond lengths in the range of 2.05–2.32 Å, while group $Fe^{II}O_6$ has a broader range of bond length (2.05–2.51 Å). However, the average Fe–O bond length of the two types of FeO_6 octahedra are almost identical. The degree of distortion Δ can be estimated according to Formula (2) [12]

$$\Delta = \frac{1}{6}\sum_{n=1,6}\frac{d_n - \langle d\rangle}{\langle d\rangle} \quad (2)$$

where d_n and $\langle d\rangle$ are the particular and average Fe–O bond lengths. The groups $Fe^{II}O_6$ have a larger distortion value than the groups $Fe^{I}O_6$ (5.19×10^{-3} as opposed to 1.86×10^{-3}).

Furthermore, the three nearest Fe neighbours surrounding each Na ion can be divided into three groups. The first group consists of the first nearest Fe neighbours, denoted as 1NN, with a distance of 3.513 Å to the nearest Na ion. The second group contains the second nearest Fe neighbours (2NN), 3.572 Å far away from the Na ion. The third one is the third nearest Fe neighbours, denoted as 3NN, with a longer distance of 3.724 Å. Due to the different distances, Fe ions in the groups would behave differently when the Na atom approaches or moves away.

Table 1. The lattice parameters, Fe–O bond lengths of the antiferromagnetic configuration (Å)

$Na_2Fe_3(SO_4)_4$ orthorhombic, space group $Cmc2_1$ a = 14.565 Å b = 10.035 Å c = 8.781 Å V = 1283.47 Å^3							
	O1	O2	O3	O4	O5	O6	Aver.
Fe^{I}	2.163	2.051	2.193	2.319	2.056	2.223	2.167
Fe^{II}	2.091	2.052	2.052	2.193	2.205	2.508	2.183

3.2 Electronic structure

To understand the electronic structure of the proposed material, we calculate the density of state (DOS) of $Na_2Fe_3(SO_4)_4$. As shown in Fig. 2a, $Na_2Fe_3(SO_4)_4$ exhibits the insulating behaviour with an up-spin gap/down-spin gap of 3.612/3.682 eV. The valence band is well divided into five main blocks. The first four blocks under –0.3 eV are contributed mainly by the 2*p* O states that hybridize strongly with the 2*p* S states in the region lower than –6.0 eV and with the 3*d* Fe states in the range –6.0 to –0.3 eV. While the 3*d* Fe states do not predominate the first four blocks, they hold the lion's share in the block right below

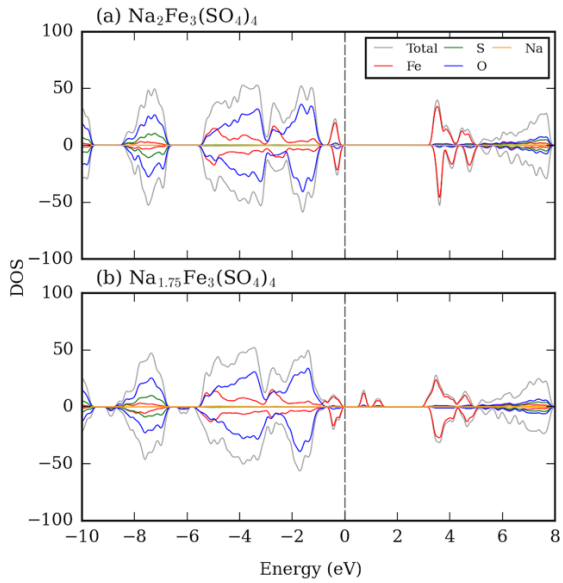

Fig. 2. Density of states of $Na_xFe_3(SO_4)_4$ structures, where x = 2 and 1.75. The Fermi level indicated by the dash line is set at 0.

pISSN 1859-1388
eISSN 2615-9678

the Fermi level, implying that the 3*d* Fe states would mainly determine the electronic conductivity of the material. Furthermore, in the conduction band, the 3*d* Fe states dominate the two first blocks while the 2*p* O and S states hold a small share in these blocks. Like $Na_2Mn_3(SO_4)_4$ [21], $Na_{2.44}Mn_{1.79}(SO_4)_3$ [31], $NaVOPO_4$ [20], and $LiFePO_4$ [13], $Na_2Fe_3(SO_4)_4$ possesses similar electronic properties in terms of the cathode material applicable for rechargeable batteries.

3.3 Average voltage

Using the formula (1), we calculate the open-circuit voltage of $Na_2Fe_3(SO_4)_4$. This material exhibits a high voltage of 4.01 V, which indicates that $Na_2Fe_3(SO_4)_4$ can be a promising cathode material applicable for rechargeable batteries. Compared with $Na_2Mn_3(SO_4)_4$ [12], $Na_2Fe_3(SO_4)_4$ possesses a slightly lower voltage. However, $Na_2Fe_3(SO_4)_4$ has a higher voltage than $NaFeO_2$ (3.3 V) [32] or $NaFePO_4$ (2.8 V) [33].

3.4 Formation of small polaron

As mentioned in the introduction section, the small polaron plays an essential role in the diffusion processes of the sodium ions in the transition metal-based cathode materials. When a sodium atom is removed from the host $Na_2Fe_3(SO_4)_4$, a positive hole would appear at a transition metal site. The strong Coulomb attraction between the positive hole and the negative anion O^{2-} causes the Fe–O bonds of a FeO_6 octahedron to shrink steadily, resulting in a local distortion at the transition metal site where the hole appears. The local distortion confines the hole inside. As a result, a small polaron is formed at the transition metal sites. In the perfect structure of $Na_2Fe_3(SO_4)_4$, three iron atoms in three FeO_6 octahedra surround each Na ion. The iron atoms can be divided into three groups: first nearest neighbours (1NN), second nearest neighbours (2NN), and third nearest neighbours (3NN). The distances from the vacancy of the sodium ion to 1NN, 2NN, and 3NN sites are 3.513, 3.572, and 3.724 Å, respectively. Therefore, when one Na vacancy is introduced to the perfect structure of $Na_2Fe_3(SO_4)_4$, three possible cases, where small polaron could be localized at one of the 1NN, 2NN, or 3NN sites, should be investigated. Among these configurations, the one with the polaron formed at the 1NN Fe site is the most preferable with lower energy ($E_{2NN} - E_{1NN}$ = 107 meV and $E_{3NN} - E_{1NN}$ = 113 meV), indicating a higher binding energy between the polaron at the 1NN Fe site and the Na vacancy.

The Fe–O bond lengths and the magnetization moment of Fe ions of the most stable configuration, where the polaron is at 1NN site, are given in Table 2. The average Fe–O bond shrinkage at the 1NN Fe site by 0.12 Å (from 2.167 Å to 2.047 Å), together with the increase in the magnitude of magnetic moment at the 1NN Fe site from 3.782 to 4.292 μ_B, confirms the polaron formation at the 1NN Fe site. Furthermore, the appearance of the bound state in the bandgap of the density of states of $Na_{1.875}Fe_3(SO_4)_4$, as shown in Fig. 2b, also provides stringent evidence to reveal the self-trapping phenomena of a hole in a local distortion.

Table 2. Fe–O bond length and magnetic moment change before and after polaron formed at 1NN site (Å)

	O1	O2	O3	O4	O5	O6	Aver.	Mag. (μ_B)
Before	2.163	2.051	2.193	2.319	2.056	2.223	2.167	3.782
After	2.12	2.008	1.990	2.205	1.982	1.975	2.047	4.292

3.5 Diffusion mechanism

To understand the ionic conductivity deeply, we investigate the diffusion mechanism of Na-vacancy in the proposed material. For this purpose, we first define all the possible elementary diffusion processes (EDPs) inside the material. Each EDP is a simultaneous diffusion process of Na vacancy and its accompanying polaron. Three typical elementary diffusion processes are single, crossing, and parallel processes [13]. The single process occurs when the accompanying polaron stays at its site during the movement of Na vacancy. The crossing or parallel processes occur when the polaron hops between two adjacent transition sites across or parallel to the Na vacancy trajectory. In this material, the single process cannot occur due to the arrangement of the Fe sites. As indicated in Fig. 3 and Fig. 4, four different EDPs between two adjacent Na-vacancy sites of $Na_2Fe_3(SO_4)_4$ can be explored from NEB calculations:

(i) Parallel process *p*1: the $[Na_1–Fe_1O_6]$ complex diffuses to the $[Na_4–Fe_4O_6]$ complex with a reaction coordinate of 6.0 Å. This process has an activation energy of 816 meV.

(ii) Parallel process *p*2: the $[Na_6–Fe_6O_6]$ complex migrates to the $[Na_8–Fe_8O_6]$ with a reaction coordinate of 8.2 Å. The activation energy of this process is at the lowest value of 808 meV.

(iii) Crossing process *c*1: the $[Na_1–Fe_1O_6]$ complex jumps to the $[Na_6–Fe_6O_6]$ complex with an activation energy of 915 meV, which is larger than one of the previous parallel processes. The trajectory of Na-vacancy also has the form of a parabola with a 7 Å distance.

(iv) Crossing process *c*2: the $[Na_1–Fe_1O_6]$ complex moves to the $[Na_8–Fe_8O_6]$ complex. The reaction coordinate is about 7.8 Å. The activation energy of this process is highest and equal to 946 meV, and this is probably the least preferable one among the four diffusion processes.

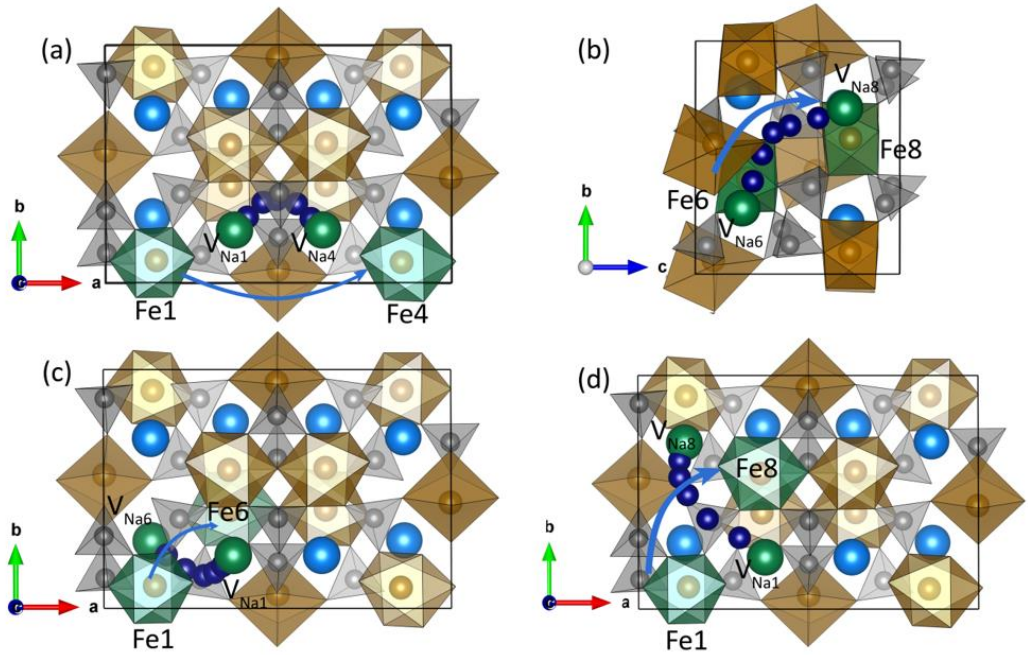

Fig. 3. Four elementary diffusion processes including parallel processes p1 (a) and p2 (b); crossing processes c1 (e) and c2 (d). The dark blue and green balls illustrate the diffusion trace of Na vacancy, initial and final position of Na vacancy. The arrows represent the polaron hopping between two green FeO_6 octahedra.

pISSN 1859-1388
eISSN 2615-9678

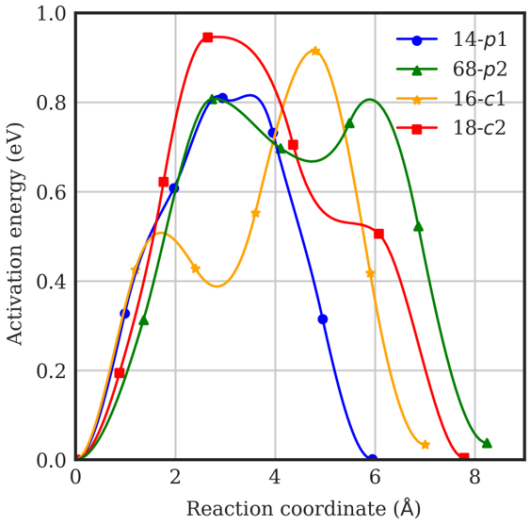

Fig. 4. Activation energy profiles with respect to reaction coordinates of four elementary diffusion processes

Obviously, *p*1 and *p*2 are more preferable diffusion processes because they have lower activation energy by 100 meV than the crossing processes. It implies that the effect of positive polaron migration on Na vacancy diffusion is substantial in the proposed material. The *p*1 and *p*2 processes have a small activation energy difference of only 8 meV, implying that both processes may occur. However, for the continuous diffusion in the whole material, the *p*1 process would proceed with combinations with the *c*1 or *c*2 process. Thus, the *p*1 process hardly occurs at a high Na regime while the *p*2 process is preferable. Consequently, the favourable diffusion pathway would be a combination with the *p*2 process, as illustrated by the zigzag-like trajectory along the [001] direction in Fig. 5.

The proposed material exhibits slightly lower activation energy than $Na_2Mn_3(SO_4)_4$, indicating that this proposed material may have a slightly higher ionic conductivity than $Na_2Mn_3(SO_4)_4$. Besides, in both $Na_2Mn_3(SO_4)_4$ and $Na_2Fe_3(SO_4)_4$, the Na vacancy favourably diffuses in a one-dimensional pathway along the [001] direction.

4 Conclusion

The crystal structure, electronic structure, voltage, and the diffusion mechanism of a new cathode material $Na_2Fe_3(SO_4)_4$ are systematically investigated. The proposed material exhibits a high open-circuit voltage of about 4.0 V and an activation energy of 808 meV for the Na ion diffusion and can be expected as a promising candidate for cathode materials.

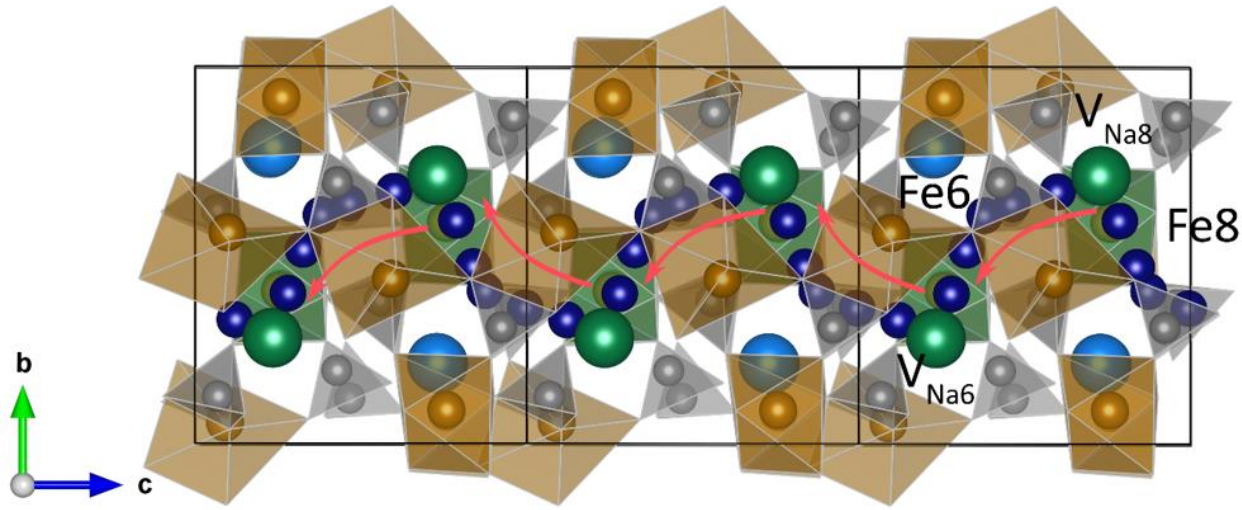

Fig. 5. The most preferable diffusion pathway along the [001] direction

DOI: 10.26459/hueunijns.v130i1B.6190

Funding statement

This research is funded by Vietnam National Foundation for Science and Technology Development (NAFOSTED) under grant number 103.01-2020.44.

Acknowledgement

This work is supported by the Vietnam Project on the Establishment of the Master's in Nanotechnology Program of Vietnam-Japan University under the contract between Japan International Cooperation Agency (JICA) and Osaka University.

References

1. Kavanagh L, Keohane J, Garcia Cabellos G, Lloyd A, Cleary J. Global lithium sources—industrial use and future in the electric vehicle industry: A review. Resources. 2018;7(3):57.
2. Delmas C, Braconnier J-J, Fouassier C, Hagenmuller P. Electrochemical intercalation of sodium in Na_xCoO_2 bronzes. Solid State Ionics. 1981 08;3-4:165-169.
3. Fleischer M. The abundance and distribution of the chemical elements in the earth's crust. Journal of Chemical Education. 1954;31(9):446.
4. Zhu Y, Xu Y, Liu Y, Luo C and Wang C. Comparison of electrochemical performances of olivine $NaFePO_4$ in sodium-ion batteries and olivine $LiFePO_4$ in lithium-ion batteries. Nanoscale. 2013;5(2):780-787.
5. Okada S, Takahashi Y, Kiyabu T, Doi T, Yamaki J, Nishida T. Layered transition metal oxides as cathodes for sodium secondary battery. ECS Meeting Abstracts. 2006.
6. Yabuuchi N, Kajiyama M, Iwatate J, Nishikawa H, Hitomi S, Okuyama R, et al. P2-type $Na_x[Fe_{1/2}Mn_{1/2}]O_2$ made from earth-abundant elements for rechargeable Na batteries. Nature Materials. 2012;11(6):512-517.
7. EllisBL, Makahnouk WRM, Makimura Y, Toghill K, Nazar LF. A multifunctional 3.5 V iron-based phosphate cathode for rechargeable batteries. Nature Materials. 2007;6(10):749-753.
8. Tang W, Song X, Du Y, Peng C, Lin M, Xi S, et al. High-performance $NaFePO_4$ formed by aqueous ion-exchange and its mechanism for advanced sodium ion batteries. Journal of Materials Chemistry A. 2016;4(13):4882-4892.
9. Barpanda P, Ye T, Nishimura S-i, Chung S-C, Yamada Y, Okubo M, et al. Sodium iron pyrophosphate: A novel 3.0 V iron-based cathode for sodium-ion batteries. Electrochemistry Communications. 2012;24:116-119.
10. Kim H, Park I, Seo D-H, Lee S, Kim S-W, Kwon WJ, et al. New iron-based mixed-polyanion cathodes for lithium and sodium rechargeable batteries: combined first principles calculations and experimental study. Journal of the American Chemical Society. 2012 06 14;134(25):10369-10372.
11. Barpanda P, Oyama G, Ling CD, Yamada A. Kröhnkite-Type $Na_2Fe(SO_4)_2{\cdot}2H_2O$ as a novel 3.25 V insertion compound for Na-ion batteries. Chemistry of Materials. 2014;26(3):1297-1299.
12. Gao J, Sha X, Liu X, Song L, Zhao P. Preparation, structure and properties of $Na_2Mn_3(SO_4)_4$: a new potential candidate with high voltage for Na-ion batteries. Journal of Materials Chemistry A. 2016;4(30):11870-11877.
13. Dinh VA, Nara J, Ohno T. A New Insight into the Polaron–Li Complex Diffusion in Cathode Material $LiFe_{1-y}Mn_yPO_4$ for Li Ion Batteries. Applied Physics Express. 2012;5(4):045801.
14. Bui KM, Dinh VA, Ohno T. Diffusion Mechanism of Polaron–Li Vacancy Complex in Cathode Material Li_2FeSiO_4. Applied Physics Express. 2012;5(12):125802.
15. Duong DM, Dinh VA, Ohno T. Quasi-Three-Dimensional Diffusion of Li ions in $Li_3FePO_4CO_3$: First-Principles Calculations for Cathode Materials of Li-Ion Batteries. Applied Physics Express. 2013;6(11):115801.
16. Bui KM, Dinh VA, Okada S, Ohno T. Hybrid functional study of the NASICON-type $Na_3V_2(PO_4)_3$: crystal and eletronic structures and polaron-Na vacancy complex diffusion. Physical Chemistry Chemical Physics. 2015;17(45):30433-30439.
17. Bui KM, Dinh VA, Okada S, Ohno T. Na-ion diffusion in a NASICON-type solid electrolyte: a density functional study. Physical Chemistry Chemical Physics. 2016;18(39):27226-27231.

pISSN 1859-1388
eISSN 2615-9678

18. Debbichi M, Debichi N, Dinh VA, Lebegue S. First principles study of the crystal, electronic structure, and diffusion mechanism of polaron-Na vacancy of $Na_3MnPO_4CO_3$ for Na-ion battery applications. Journal of Physics D: Applied Physics. 2016;50(4):045502.

19. Luong HD, Pham TD, Morikawa Y, Shibutani Y, Dinh VA. Diffusion mechanism of Na ion–polaron complex in potential cathode materials $NaVOPO_4$ and $VOPO_4$ for rechargeable sodium-ion batteries. Physical Chemistry Chemical Physics. 2018;20(36):23625-23634.

20. Tran TL, Luong HD, Duong DM, Dinh NT, Dinh VA. Hybrid functional study on small polaron formation and ion diffusion in the cathode material $Na_2Mn_3(SO_4)_4$. ACS Omega. 2020;5(10):5429-5435.

21. Luong HD, Dinh VA, Momida H, Oguchi T. Insight into the diffusion mechanism of sodium ion – polaron complexes in orthorhombic P2 layered cathode oxide Na_xMnO_2. Physical Chemistry Chemical Physics. 2020;22(32):18219-18228.

22. Kresse G, Hafner J. Ab initio molecular dynamics for open-shell transition metals. Physical Review B. 1993;48(17):13115-13118.

23. Kresse G, Joubert D. From ultrasoft psuedopotentials to the projector augmented-wave method. Physical Review B. 1999;59(3):1758-1775.

24. Kresse G, Hafner J. Norm-conserving and ultrasoft pseudopotentials for first-row and transition elements. Journal of Physics: Condensed Matter. 1994;6(40):8245-8257.

25. Kresse G, Furthmuller J. Efficiency of Ab initio total energy calculations for metals and semiconductors using a plane-wave basis set. Computational Materials Science. 1996 07;6(1):15-50.

26. Perdew J, Burke K, Ernzerhof M. Generalized gradient approximation made simple. Physical Review Letters. 1996;77(18):3865-3868.

27. Wang L, Maxisch T, Ceder G. Oxidation energies of transition metal oxides within the GGA+U framework. Physical Review B. 2006;73(19).

28. Togo A, Tanaka I. First principles phonon calculations in materials science. Scripta Materialia. 2015;108:1-5.

29. Pick RM, Cohen MH, Martin RM. Microscopic theory of force constants in the adiabatic approximation. Physical Review B. 1970;1(2):910-920.

30. Henkelman G, Jónsson H. Improved tangent estimate in the nudged elastic band method for finding minimum energy paths and saddle points. The Journal of Chemical Physics. 2000;113(22):9978-9985.

31. Dwibedi D, Araujo RB, Chakraborty S, Shanbogh PP, Sundaram NG, Ahuja R. $Na_{2.44}Mn_{1.79}(SO_4)_3$: a new member of the alluaudite family of insertion compounds for sodium ion batteries. Journal of Materials Chemistry A. 2015;3(36):18564-18571.

32. Zhao J, Zhao L, Dimov N, Okada S, Nishida T. Electrochemical and thermal properties of α-$NaFeO_2$ cathode for Na-ion batteries. Journal of The Electrochemical Society. 2013;160(5):A3077-A3081.

33. Wongittharom N, Lee T-C, Wang C-H, Wang Y-C, Chang J-K. Electrochemical performance of $Na/NaFePO_4$ sodium-ion batteries with ionic liquid electrolytes. Journal of Materials Chemistry A. 2014;2(16):5655.